J. Plasma Physics (2006), *vol.* 72, *part* 3, *pp.* 341–349.
doi:10.1017/S0022377805004058 First published online 25 November 2005 Printed in the United Kingdom

Chaotic electron trajectories in a free-electron laser with helical wiggler and ion-channel guiding

MOHAMMAD S. FALLAH[1], MAHDI ESMAEILZADEH[1], JOSEPH E. WILLETT[2] and LORI J. WILLETT[3]

[1]Department of Physics, Iran University of Science and Technology, Tehran, Iran
(mahdi@iust.ac.ir)

[2]Department of Physics and Astronomy, University of Missouri-Columbia, Columbia, MO 65211, USA
(willettje@missouri.edu)

[3]Department of Mathematics, University of New Orleans, New Orleans, LA 70148, USA

(Received 20 January 2005 and in accepted form 1 March 2005)

Abstract. An analysis of relativistic electron trajectories in a free-electron laser with a helical magnetic wiggler and an ion channel is presented. The wiggler field amplitude and the ion number density are taken to be uniform. Also included are the self-electric and self-magnetic fields of the electron beam, which is assumed to be of constant velocity and electron number density. The Hamiltonian, which is a constant of the motion, is first expressed in cartesian coordinates and momenta. A second constant of the motion is obtained by canonical transformation. The steady-state orbits, Poincaré maps, and Liapunov exponents are employed to investigate the chaotic motion in the presence of the ion channel. Numerical calculations reveal conditions under which chaotic and non-chaotic orbits exist.

1. Introduction

The motion of a single relativistic electron in a constant-amplitude helical wiggler magnetic field and uniform axial magnetic field has been analyzed extensively in the literature. This is a valid approximation for an electron beam in a low-wiggler-amplitude, low-current, free-electron laser (FEL). In this case, the electrostatic and magnetic self-fields produced by the beam space charge and current may be neglected. The motion of a test electron is then integrable and non-chaotic. An analysis of the effects of the electric and magnetic self-fields has been carried out by Chen and Davidson [1] and by Michel et al. [2]. It was shown that the motion is non-integrable. Consequently, part of the phase space becomes chaotic in the sense that adjacent initial conditions lead to exponentially divergent trajectories. If the self-fields are sufficiently strong, the group I and group II orbits can become fully chaotic.

The effects of non-uniformity of the wiggler field amplitude in addition to the self-fields of the electron beam were analyzed by Spindler and Renz [3]. Both of these effects were shown to yield chaotic motion. Their study indicated that, near magnetoresonance, surprisingly low beam currents can induce chaotic motion.

With high axial guide fields, the wiggler-amplitude non-uniformity had little effect because the orbits were confined near the central axis. With moderate guide fields, the non-uniformity became important and the self-fields had very little effect. Chaotic electron dynamics in planar wiggler magnetic fields have also been studied [2, 4].

It has been suggested that the passage of an electron beam through an ion channel may provide an alternative to the use of an axial magnetic guide field. Several theoretical studies indicate that ion-channel guiding may offer some distinct advantages; see, e.g., [5,6]. In Sec. 2 of the present paper, the relativistic motion of a test electron in a FEL with helical wiggler and ion channel is formulated. An idealized wiggler magnetic field of constant amplitude and an electrostatic field due to positive ions of constant number density and introduced. The self-electric and self-magnetic fields of the electron beam of constant number density and velocity are also included. The time-independent Hamiltonian (total energy) is constructed in terms of cartesian coordinates and momenta, and comprises a constant of the motion. By a canonical transformation, it is expressed in new variables and a second constant of the motion is identified. The steady-state solution of the equation of motion is then derived in cartesian coordinates and two groups of electron orbits are defined.

In Sec. 3, the steady-state orbits, Poincaré maps and Liapunov exponents are employed to investigate the chaotic behavior of the motion. A graph of the axial velocity versus ion-channel plasma frequency is shown in Fig. 1 and the regions in which each orbit group exists are illustrated. Figures 2–4 are Poincaré surface-of-section plots for three selected ion-channel plasma frequencies. They show that, for certain values of the frequency, the motion is chaotic or regular. Figure 5 confirms by use of Liapunov exponents the chaotic and non-chaotic motion.

2. Theoretical model and assumptions

In a high-current (high-density) beam, the motion of a test electron in a FEL with helical wiggler and ion-channel guiding can be altered significantly by the self-electric and self-magnetic fields induced by the beam space charge and current, respectively. In order to model the self-fields of the electron beam, we make the assumption of a homogenous electron density profile

$$n_{\mathrm{b}}(r) = \begin{cases} n_{\mathrm{b}} = \text{constant} & \text{for } r \leqslant r_{\mathrm{b}}, \\ 0 & \text{for } r > r_{\mathrm{b}}, \end{cases} \tag{1}$$

where n_{b} is the number density of the beam electrons and r_{b} is the radius of the beam. In addition, the electron beam is assumed to have uniformal axial current density

$$\mathbf{J}_{\mathrm{b}} = -en_{\mathrm{b}}c\beta_{\mathrm{b}}\hat{\mathbf{e}}_z \tag{2}$$

over the radial cross section of the electron beam. Here $-e$ is the electron charge, c is the speed of light in a vacuum, and β_{b} is the normalized average axial velocity of the electron beam. With these assumptions, the self-electric and self-magnetic fields of the electron in the interior of the beam ($r \leqslant r_{\mathrm{b}}$) are given in [7]

$$\mathbf{E}_{\mathrm{s}} = -2\pi en_{\mathrm{b}}(x\hat{\mathbf{e}}_x + y\hat{\mathbf{e}}_y) \tag{3}$$

and

$$\mathbf{B}_{\mathrm{s}} = 2\pi en_{\mathrm{b}}\beta_{\mathrm{b}}(y\hat{\mathbf{e}}_x - x\hat{\mathbf{e}}_y), \tag{4}$$

respectively.

https://doi.org/10.1017/S0022377805004058 Published online by Cambridge University Press

The magnetic field of an idealized helical wiggler may be described by

$$\mathbf{B}_{\mathrm{w}} = B_{\mathrm{w}}\lfloor \hat{\mathbf{e}}_x \cos(k_{\mathrm{w}} z) + \hat{\mathbf{e}}_y \sin(k_{\mathrm{w}} z)\rfloor, \tag{5}$$

where B_{w} is the wiggler amplitude and k_{w} is the wiggler wave number. The transverse electrostatic field generated by an ion channel can be written as

$$\mathbf{E}_{\mathrm{i}} = 2\pi e n_{\mathrm{i}}(x\hat{\mathbf{e}}_x + y\hat{\mathbf{e}}_y), \tag{6}$$

where n_{i} is the density of positive ions having charge $+e$. Taking into account the self-fields, the Hamiltonian of a test relativistic electron in the combined wiggler and ion-channel fields becomes

$$\mathrm{H} = [(c\mathbf{P} + e\mathbf{A})^2 + m^2c^4]^{1/2} + e(\phi_{\mathrm{i}} - \phi_{\mathrm{s}}) \equiv \gamma mc^2 + e(\phi_{\mathrm{i}} - \phi_{\mathrm{s}}), \tag{7}$$

where $\mathbf{P}$ is the canonical momentum, m is the electron rest mass, γ is the relativistic factor,

$$\mathbf{A} \equiv \frac{B_{\mathrm{w}}}{k_{\mathrm{w}}}[\hat{\mathbf{e}}_x \cos(k_{\mathrm{w}} z) + \hat{\mathbf{e}}_y \sim (k_{\mathrm{w}} z)] + \beta_{\mathrm{b}}\phi_{\mathrm{s}}\hat{\mathbf{e}}_z \tag{8}$$

is the vector potential, and

$$\phi_{\mathrm{i}} \equiv -\frac{m\omega_{\mathrm{i}}^2}{4e}(x^2 + y^2) \tag{9}$$

and

$$\phi_{\mathrm{s}} \equiv \frac{m\omega_{\mathrm{b}}^2}{4e}(x^2 + y^2) \tag{10}$$

are the electrostatic potentials due to the ion channel and electron beam, respectively. In (9) and (10), $\omega_{\mathrm{i}} \equiv (4\pi e^2 n_{\mathrm{i}}/m)^{1/2}$ and $\omega_{\mathrm{b}} \equiv (4\pi e^2 n_{\mathrm{b}}/m)^{1/2}$ are the nonrelativistic plasma frequencies of the ion channel and electron beam, respectively.

As the Hamiltonian (7) is not an explicit function of time, H is a constant of motion, i.e.

$$\mathrm{H} = \gamma mc^2 + e(\phi_{\mathrm{i}} - \phi_{\mathrm{s}}) = \text{constant}, \tag{11}$$

which corresponds to the conservation of total energy. For numerical calculations, we introduce the following normalized (dimensionless) parameters and variables:

$$\begin{gathered}
\bar{\mathrm{H}} \equiv \frac{\mathrm{H}}{mc^2}, \quad \bar{\mathbf{P}} \equiv \frac{\mathbf{P}}{mc}, \quad \bar{\mathbf{A}} \equiv \frac{e\mathbf{A}}{mc^2}, \\
\bar{\phi}_{\mathrm{i}} \equiv \frac{e\phi_{\mathrm{i}}}{mc^2}, \quad \bar{\phi}_{\mathrm{s}} \equiv \frac{e\phi_{\mathrm{s}}}{mc^2}, \quad \bar{\omega}_{\mathrm{i}} \equiv \frac{e\omega_{\mathrm{i}}}{k_{\mathrm{w}}c}, \quad \bar{\omega}_{\mathrm{b}} \equiv \frac{\omega_{\mathrm{b}}}{k_{\mathrm{w}}c}, \\
\bar{x} \equiv k_{\mathrm{w}}x, \quad \bar{y} \equiv k_{\mathrm{w}}y, \quad \bar{z} \equiv k_{\mathrm{w}}z, \\
\alpha_{\mathrm{w}} \equiv \frac{e\mathbf{B}_{\mathrm{w}}}{mk_{\mathrm{w}}c^2}, \quad \tau \equiv k_{\mathrm{w}}ct,
\end{gathered} \tag{12}$$

where t is time and α_{w} is a measure of the wiggler magnetic field amplitude. Using (12), the Hamiltonian in the normalized form can be written as

$$\bar{\mathrm{H}} \equiv [(\bar{\mathbf{P}}_x + \alpha_{\mathrm{w}}\cos\bar{z})^2 + (\bar{\mathbf{P}}_y + \alpha_{\mathrm{w}}\sin\bar{z})^2 + (\bar{\mathbf{P}}_z + \beta_{\mathrm{b}}\bar{\phi}_{\mathrm{s}})^2 + 1]^{1/2} + \bar{\phi}_{\mathrm{i}} - \bar{\phi}_{\mathrm{s}}, \tag{13}$$

where the normalized ion-channel and electron-beam potentials are defined by

$$\bar{\phi}_{\mathrm{i}} \equiv -\frac{\bar{\omega}_{\mathrm{i}}^2}{4}(\bar{x}^2 + \bar{y}^2) \tag{14}$$

https://doi.org/10.1017/S0022377805004058 Published online by Cambridge University Press

and

$$\bar{\phi}_{\rm s} \equiv -\frac{\bar{\omega}_{\rm b}^2}{4}(\bar{x}^2 + \bar{y}^2), \tag{15}$$

respectively. As mentioned before, the Hamiltonian is independent of time. Thus, the total energy is a constant of the motion. In order to find an additional constant of the motion, the canonical transformation to the new variables $(\phi, \psi, z', \mathbf{P}_\varphi, \mathbf{P}_\psi, \mathbf{P}_{z'})$ defined by

$$\bar{x} \equiv -\sqrt{\mathbf{P}_\phi}\cos(\phi - z') + \sqrt{\mathbf{P}_\psi}\sin(\psi + z'), \tag{16}$$

$$\bar{y} \equiv \sqrt{\mathbf{P}_\phi}\sin(\phi - z') - \sqrt{\mathbf{P}_\psi}\cos(\psi + z'), \tag{17}$$

$$\bar{z} \equiv z', \tag{18}$$

$$\bar{\mathbf{P}}_x \equiv \sqrt{\mathbf{P}_\phi}\sin(\phi - z') + \sqrt{\mathbf{P}_\psi}\cos(\psi + z'), \tag{19}$$

$$\bar{\mathbf{P}}_y \equiv \sqrt{\mathbf{P}_\phi}\cos(\phi - z') + \sqrt{\mathbf{P}_\psi}\sin(\psi + z'), \tag{20}$$

$$\bar{\mathbf{P}}_z \equiv \mathbf{P}_{z'} - \mathbf{P}_\psi + \mathbf{P}_\phi \tag{21}$$

is introduced. The normalized Hamiltonian in the new variables can be written as

$$\bar{\rm H} = [\mathbf{P}_\phi + \mathbf{P}_\psi + 2\sqrt{\mathbf{P}_\phi \mathbf{P}_\psi}\sin(\phi + \psi) + 2\alpha_{\rm w}(\sqrt{\mathbf{P}_\phi}\sin\phi + \sqrt{\mathbf{P}_\psi}\cos\psi) + \alpha_{\rm w}^2 + \mathbf{P}_z^2 + 1]^{1/2} + \bar{\phi}_{\rm i} - \bar{\phi}_{\rm s}, \tag{22}$$

where

$$\mathbf{P}_z \equiv \mathbf{P}_{z'} - \mathbf{P}_\psi + \mathbf{P}_\phi + \beta_{\rm b}\bar{\phi}_{\rm s} \tag{23}$$

is the axial mechanical momentum, and

$$\bar{\phi}_{\rm i} \equiv -\frac{\bar{\omega}_{\rm i}^2}{4}[\mathbf{P}_\phi + \mathbf{P}_\psi - 2\sqrt{\mathbf{P}_\phi \mathbf{P}_\psi}\sin(\phi + \psi)] \tag{24}$$

and

$$\bar{\phi}_{\rm s} \equiv -\frac{\bar{\omega}_{\rm b}^2}{4}[\mathbf{P}_\phi + \mathbf{P}_\psi - 2\sqrt{\mathbf{P}_\phi \mathbf{P}_\psi}\sin(\phi + \psi)] \tag{25}$$

are the normalized ion-channel and electron-beam potentials after transformation. Since the Hamiltonian in (22) is not an explicit function of z', it follows that $\mathbf{P}_{z'}$ is another constant of the motion.

Having failed in finding a third constant of the motion, Poincaré maps and Liapunov exponents have been used to investigate the chaotic behavior of the motion. Using the Hamiltonian defined by (22), the equations of motion can be written in the form

$$\dot{\phi} = \frac{1}{2\mathbf{K}}\left\{\frac{\alpha_{\rm w}}{\mathbf{P}_\phi^{1/2}}\sin\phi + 2\mathbf{P}_z\left[1 + \frac{1}{4}\beta_{\rm b}\bar{\omega}_{\rm b}^2(1 - \mathbf{M})\right] + 1 + \mathbf{M}\right\} + \left(\frac{\bar{\omega}_{\rm i}^2 - \bar{\omega}_{\rm b}^2}{4}\right)(1 - \mathbf{M}), \tag{26}$$

$$\dot{\psi} = \frac{1}{2\mathbf{K}}\left\{\frac{\alpha_{\rm w}}{\mathbf{P}_\phi^{1/2}}\cos\psi - 2\mathbf{P}_z\left[1 - \frac{1}{4}\beta_{\rm b}\bar{\omega}_{\rm b}^2\left(1 - \mathbf{M}\frac{\mathbf{P}_\phi}{\mathbf{P}_\psi}\right)\right] + 1 + \mathbf{M}\frac{\mathbf{P}_\phi}{\mathbf{P}_\psi}\right\} + \left(\frac{\bar{\omega}_{\rm i}^2 - \bar{\omega}_{\rm b}^2}{4}\right)\left(1 - \mathbf{M}\frac{\mathbf{P}_\phi}{\mathbf{P}_\psi}\right), \tag{27}$$

https://doi.org/10.1017/S0022377805004058 Published online by Cambridge University Press

$$\dot{\mathbf{P}}_\phi = \frac{1}{\mathbf{K}}\left[\mathbf{N}\left(1-\frac{1}{4}\beta_\mathrm{b}\bar{\omega}_\mathrm{b}^2\mathbf{P}_z\right)+\alpha_\mathrm{w}\mathbf{P}_\phi^{1/2}\cos\phi\right]-\frac{1}{2}\mathbf{N}(\bar{\omega}_\mathrm{i}^2-\bar{\omega}_\mathrm{b}^2), \tag{28}$$

$$\dot{\mathbf{P}}_\psi = \frac{1}{\mathbf{K}}\left[\mathbf{N}\left(1-\frac{1}{4}\beta_\mathrm{b}\bar{\omega}_\mathrm{b}^2\mathbf{P}_z\right)-\alpha_\mathrm{w}\mathbf{P}_\psi^{1/2}\sin\psi\right]-\frac{1}{2}\mathbf{N}(\bar{\omega}_\mathrm{i}^2-\bar{\omega}_\mathrm{b}^2), \tag{29}$$

where

$$\mathbf{K} \equiv [(1+2\mathbf{M})\mathbf{P}_\phi + \mathbf{P}_\psi + 2\alpha_\mathrm{w}(\mathbf{P}_\phi^{1/2}\sin\phi + \mathbf{P}_\psi^{1/2}\cos\psi) + \alpha_\mathrm{w}^2 + \mathbf{P}_z^2 + 1]^{1/2} \tag{30}$$

and

$$\mathbf{M} \equiv \left(\frac{\mathbf{P}_\psi}{\mathbf{P}_\phi}\right)^{1/2}\sin(\phi+\psi), \tag{31}$$

and

$$\mathbf{N} \equiv (\mathbf{P}_\phi\mathbf{P}_\psi)^{1/2}\cos(\phi+\psi). \tag{32}$$

Before solving these equations numerically, we study the steady-state orbits in the presence of the self-fields by the Lorentz force equations

$$\frac{d\mathbf{P}}{dt} = -e\left(\mathbf{E}+\frac{1}{c}\,\mathbf{v}\times\mathbf{B}\right), \tag{33}$$

where $\mathbf{P} \equiv m\gamma\mathbf{v}$ is the relativistic momentum, and

$$\mathbf{E} = \mathbf{E}_\mathrm{i} + \mathbf{E}_\mathrm{s} \tag{34}$$

and

$$\mathbf{B} = \mathbf{B}_\mathrm{w} + \mathbf{B}_\mathrm{s} \tag{35}$$

are the total electric and magnetic fields, respectively. Using (3)–(6), the equation of motion (33) can be written in the scalar form:

$$\frac{d\beta_x}{dt} = -\frac{ck_\mathrm{w}}{2\gamma}\{k_\mathrm{w}[\bar{\omega}_\mathrm{i}^2-\bar{\omega}_\mathrm{b}^2(1-\beta_z^2)]x - 2\alpha_\mathrm{w}\beta_z\sin(k_\mathrm{w}z)\}, \tag{36}$$

$$\frac{d\beta_y}{dt} = -\frac{ck_\mathrm{w}}{2\gamma}\{k_\mathrm{w}[\bar{\omega}_\mathrm{i}^2-\bar{\omega}_\mathrm{b}^2(1-\beta_z^2)]y + 2\alpha_\mathrm{w}\beta_z\cos(k_\mathrm{w}z)\}, \tag{37}$$

$$\frac{d\beta_z}{dt} = \frac{ck_\mathrm{w}}{2\gamma}\{k_\mathrm{w}\bar{\omega}_\mathrm{b}^2(x\beta_x+y\beta_y) + 2\alpha_\mathrm{w}[\beta_y\cos(k_\mathrm{w}z)-\beta_x\sin(k_\mathrm{w}z)]\}. \tag{38}$$

The steady-state solution of (36)–(38) for the normalized velocity components may be written as

$$\beta_x = \frac{2\alpha_\mathrm{w}\beta_\parallel^2}{\bar{\omega}_\mathrm{i}^2-\bar{\omega}_\mathrm{b}^2(1-\beta_\parallel^2)-2\gamma\beta_\parallel^2}\cos(k_\mathrm{w}z), \tag{39}$$

$$\beta_y = \frac{2\alpha_\mathrm{w}\beta_\parallel^2}{\bar{\omega}_\mathrm{i}^2-\bar{\omega}_\mathrm{b}^2(1-\beta_\parallel^2)-2\gamma\beta_\parallel^2}\sin(k_\mathrm{w}z), \tag{40}$$

$$\beta_z \equiv \beta_\parallel = \text{constant}. \tag{41}$$

Equations (39) and (40) show a resonant enhancement in the magnitude of the transverse electron velocity when

$$\bar{\omega}_\mathrm{i} = [\bar{\omega}_\mathrm{b}^2(1-\beta_\parallel^2)-2\gamma\beta_\parallel^2]^{1/2}, \tag{42}$$

https://doi.org/10.1017/S0022377805004058 Published online by Cambridge University Press

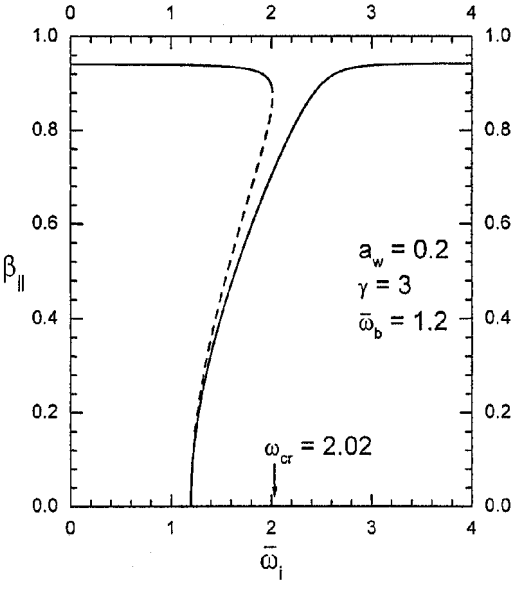

Figure 1. A graph of the normalized axial velocity of the steady-state orbits as a function of the normalized ion-channel plasma frequency. The solid (dashed) lines correspond to the stable (unstable) orbits.

which separates the electron orbits into two groups. Group I and group II are defined by

$$\bar{\omega}_i < [\bar{\omega}_b^2(1-\beta_\parallel^2) - 2\gamma\beta_\parallel^2]^{1/2} \tag{43}$$

and

$$\bar{\omega}_i > [\bar{\omega}_b^2(1-\beta_\parallel^2) - 2\gamma\beta_\parallel^2]^{1/2}, \tag{44}$$

respectively. The normalized axial velocity for steady-state trajectories is obtained from the conservation of energy. This yields

$$\beta_\parallel^2\left\{1+\left[\frac{2\alpha_w\beta_\parallel}{\bar{\omega}_i^2-\bar{\omega}_b^2(1-\beta_\parallel^2)-2\gamma\beta_\parallel^2}\right]^2\right\}+\gamma^{-2}-1=0. \tag{45}$$

There are in general six solutions for $\beta_\parallel$ for any set of parameters; only the three for which $\beta_\parallel > 0$ will be considered here.

3. Numerical results and discussion

A numerical study of the chaotic behavior of electron motion in combined wiggler magnetic and ion-channel electric fields has been made. The steady-state orbits and Poincaré maps have been computed using (45) and (26)–(29), respectively. The normalized wiggler field amplitude α_w was taken to be 0.2, the normalized beam plasma frequency $\bar{\omega}_b$ was taken to be 1.2 and the relativistic factor γ was taken to be 3. The graph of the normalized axial velocity $\beta_\parallel$ as a function of the normalized ion-channel plasma frequency $\bar{\omega}_i$ is shown in Fig. 1. The dashed line indicates the unstable branch of the group I orbits. Group I and group II orbits are defined by (43) and (44), respectively. As this figure shows, for the region $0 \leqslant \bar{\omega}_i < \bar{\omega}_b$ ($\bar{\omega}_b = 1.2$) only group I orbits exist and for the region $\bar{\omega}_i > \bar{\omega}_{cr}$ ($\bar{\omega}_{cr} \cong 2.01$) only group II orbits

https://doi.org/10.1017/S0022377805004058 Published online by Cambridge University Press

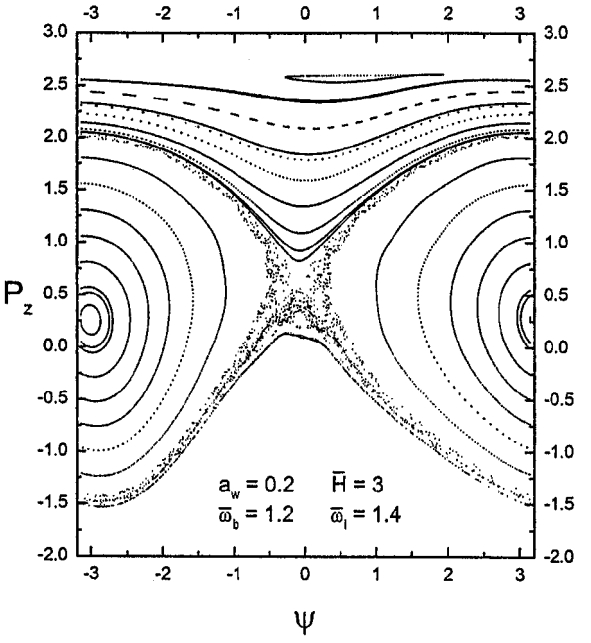

Figure 2. A Poincaré non-integrable surface-of-section plot in the $(\psi, \mathbf{P}_z)$ plane at $\phi = 0 \pmod{2\pi}$ for ion-channel plasma frequency $\bar{\omega}_\mathrm{i} = 1.4$.

exist, whereas for the region $\bar{\omega}_\mathrm{b} \leqslant \bar{\omega}_\mathrm{i} \leqslant \bar{\omega}_\mathrm{cr}$ both group I and group II orbits exists. Note that the last region ($\bar{\omega}_\mathrm{b} \leqslant \bar{\omega}_\mathrm{i} \leqslant \bar{\omega}_\mathrm{cr}$) is near the ion-channel resonance region.

Poincaré surface-of-section maps have been generated by numerically integrating the equations of motion (26)–(29). A fourth-order Runge–Kutta method with adaptive step size has been used to integrate the equations of motion. The Henon method [8] has also been used to obtain accurately the intersection of a trajectory with a surface of motion obtained from (26)–(29). This motion occurs in a three-dimensional space $(\phi, \psi, \bar{\mathrm{P}}_\varphi)$. Note that $\bar{\mathrm{P}}_\psi$ is determined from $\bar{\mathrm{H}} =$ constant. The plane (ψ, P_z) with $\phi = 0 \pmod{2\pi}$ is chosen to be the surface-of-section. The normalized total energy $\bar{\mathrm{H}}$ was taken to be 3 and the normalized beam average axial velocity β_b was taken to be 0.93. Figure 2 shows a Poincaré surface-of-section plot for normalized ion-channel group I orbits because $\bar{\omega}_\mathrm{i} = 0.9 < \bar{\omega}_\mathrm{b}$ and all trajectories shown in Fig. 4 correspond to group II orbits since $\bar{\omega}_\mathrm{i} = 2.5 > \bar{\omega}_\mathrm{cr}$. Note that $\bar{\omega}_\mathrm{i} = 1.4$ (Fig. 2) lies in the ion-channel resonance region, and $\bar{\omega}_\mathrm{i} = 0.9$ (Fig. 3) and $\bar{\omega}_\mathrm{i} = 2.5$ (Fig. 4) are far enough from ion-channel resonance. Therefore it is an interesting result that, in a FEL with helical wiggler and ion-channel guiding, the electron motion near the ion-channel resonance can be chaotic and, sufficiently far from the ion-channel resonance, the electron motion is regular and is not chaotic.

At the end of this section we confirm the existence of chaotic motion by determining non-zero Liapunov exponents. The Liapunov exponents may be obtained by calculating the distance between two trajectories with very close initial conditions in the phase space $(x, y, z, \mathrm{P}_x, \mathrm{P}_y, \mathrm{P}_z)$. For calculating Liapunov exponents, the following initial conditions have been used:

$$\begin{aligned} &x = 0, \quad y = 0, \quad z = 1.5708, \quad \mathrm{P}_x = 1.321\,93, \quad \mathrm{P}_y = 2.25, \quad \mathrm{P}_z = 0.5, \\ &x' = 0, \quad y' = 0, \quad z' = 1.5708, \quad \mathrm{P}_{x'} = 1.322\,00, \quad \mathrm{P}_{y'} = 2.25, \quad \mathrm{P}_{z'} = 0.5. \end{aligned} \tag{46}$$

https://doi.org/10.1017/S0022377805004058 Published online by Cambridge University Press

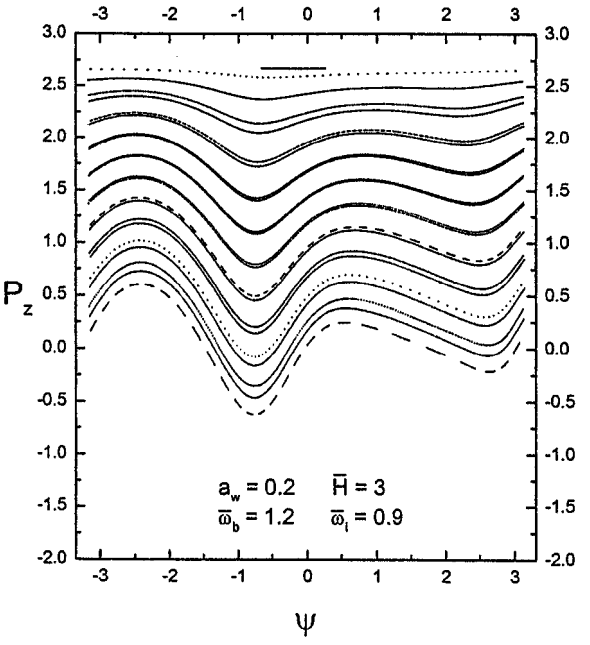

Figure 3. A Poincaré integrable surface-of-section plot in the $(\psi, \mathbf{P}_z)$ plane at $\phi = 0$ (mod 2π) for ion-channel plasma frequency $\bar{\omega}_{\rm i} = 0.9$.

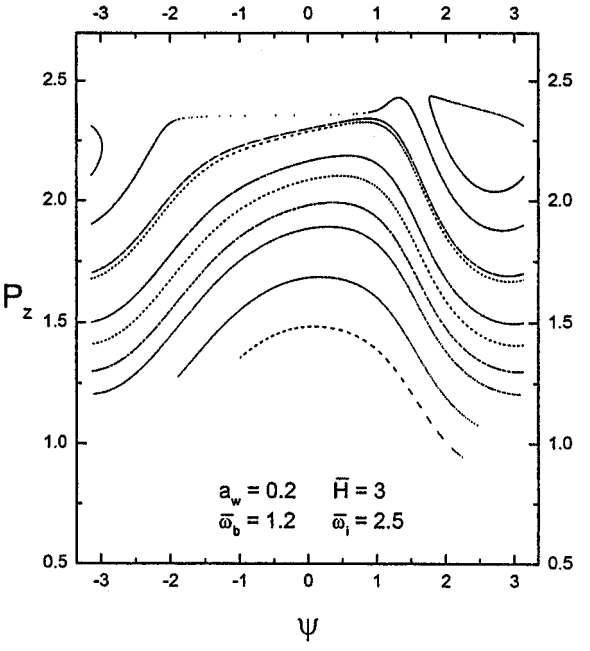

Figure 4. A Poincaré integrable surface-of-section plot in the $(\psi, \mathbf{P}_z)$ plane at $\phi = 0$ (mod 2π) for ion-channel plasma frequency $\bar{\omega}_{\rm i} = 2.5$.

https://doi.org/10.1017/S0022377805004058 Published online by Cambridge University Press

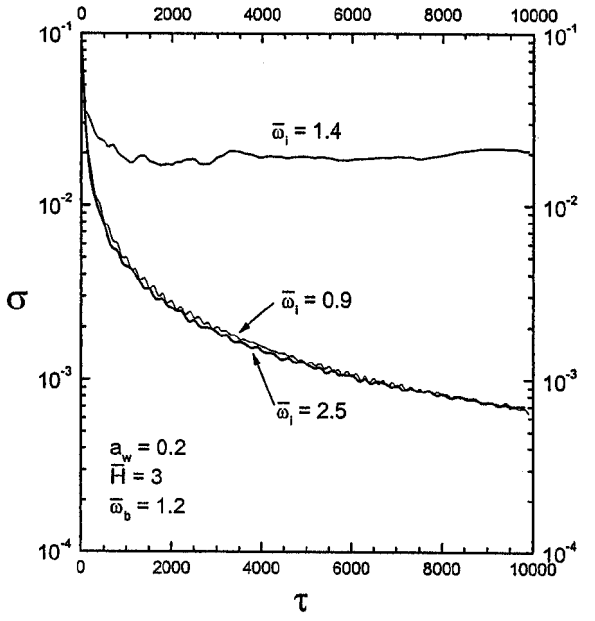

Figure 5. Liapunov exponents for ion-channel plasma frequencies $\bar{\omega}_i = 1.4$, 0.9, and 2.5 corresponding to Figs 2–4.

In Fig. 5, the Liapunov exponents corresponding to Figs 2–4 are shown. As this figure shows, for $\bar{\omega}_i = 1.4$ the Liapunov exponent remains neatly constant by increasing normalized time τ, whereas for $\bar{\omega}_i = 0.9$ and $\bar{\omega}_i = 2.5$ the Liapunov exponents tend to zero. As this figure shows, some trajectories are non-integrable and the motion can be chaotic. Here two groups (group I and group II) are allowed because $\bar{\omega}_i = 1.4$ lies in the ion-channel resonance region. In this figure, the elliptic (hyperbolic) fixed points correspond to the stable (unstable) steady-state orbits. The group I orbits have greater axial momentum than the group II orbits.

In Figs 3 and 4, Poincaré surface-of-section plots for ion-channel plasma frequencies $\bar{\omega}_i = 0.9$ and $\bar{\omega}_i = 2.5$ are shown, respectively. As these figures show, all orbits are integrable and the motion is not chaotic. All trajectories shown in Fig. 3 correspond to infinity. Therefore, Liapunov exponents confirm chaotic motion for $\bar{\omega}_i = 1.4$ and regular motion (non-chaotic) for $\bar{\omega}_i = 0.9$ and $\bar{\omega}_i = 2.5$.

References

[1] Chen, C. and Davidson, R. C. 1990 *Phys. Fluids* B **2**, 171.
[2] Michel, L., Bourdier, A. and Buzzi, J. M. 1991 *Nucl. Instrum. Methods* A **304**, 465.
[3] Spindler, G. and Renz, G. 1991 *Nucl. Instrum. Methods* A **304** 492.
[4] Chen, C. and Davidson, R. C. 1990 *Phys. Rev.* A **42**, 5041.
[5] Jha, P. and Kumar, P. 1996 *IEEE Trans. Plasma Sci.* **24**, 1354.
[6] Esmaeilzadeh, M., Mehdian, H. and Willett, J. E. 2002 *Phys. Rev.* E **65**, 016501.
[7] Esmaeilzadeh, M., Mehdian, H., Willett, J. E. and Aktas, Y. M. 2002 *Phys. Plasmas* **10**, 905.
[8] Henon, M. 1982 *Physica* D **5**, 412.

https://doi.org/10.1017/S0022377805004058 Published online by Cambridge University Press